What Do the Ultraviolet Spectra of Narrow#Line Seyfert 1 Galaxies Tell Us about Their Broad#Line Regions?

THE ASTROPHYSICAL JOURNAL, 542:692–702, 2000 October 20

WHAT DO THE ULTRAVIOLET SPECTRA OF NARROW-LINE SEYFERT 1 GALAXIES TELL US ABOUT THEIR BROAD-LINE REGIONS?

JOANNA KURASZKIEWICZ[1] AND BELINDA J. WILKES
Harvard-Smithsonian Center for Astrophysics, 60 Garden Street, Cambridge, MA 02138
BOŻENA CZERNY
Nicolaus Copernicus Astronomical Center, Warsaw, Poland
AND
SMITA MATHUR[2]
Ohio State University, Columbus, OH 43120
Received 1998 September 28; accepted 2000 June 2

ABSTRACT

We study the UV spectra of narrow-line Seyfert 1 (NLSy1) galaxies and compare them with "normal" active galactic nuclei. Similar to their optical lines, the NLSy1s show narrower UV lines. They are also characterized by weaker C IV λ1549 and C III] λ1909 and stronger Al III λ1857 emission. These UV-line properties add to the optical and X-ray properties known to be part of the Boroson & Green eigenvector 1. We show that the steep soft X-rays, which characterize the NLSy1s SEDs, change the equilibrium of the two-phase cloud-intercloud medium, resulting in somewhat higher broad-line region cloud densities, lower ionization parameter, and larger broad-line region radii. These modified conditions can explain the unusual emission-line properties we find in NLSy1. Using a specific model of an accretion disk with corona presented by Witt, Czerny, & Życki, we also show that the steep soft and hard X-ray continua can be explained if the $L/L_{\rm Edd}$ ratios are larger than in "normal" Sy1s/QSOs, strengthening earlier suggestions that the $L/L_{\rm Edd}$ is the physical parameter driving this eigenvector.

Subject headings: accretion, accretion disks — galaxies: active — galaxies: Seyfert — ultraviolet: galaxies

1. INTRODUCTION

Narrow-line Seyfert 1 galaxies (NLSy1), first suggested as a distinct class of active galactic nuclei (AGNs) by Osterbrock & Pogge (1985), are characterized by Balmer lines whose FWHM is smaller than typical Seyfert 1 galaxies, i.e., $500 < \mathrm{FWHM} < 2000$ km s^{-1}, slightly broader than the forbidden lines. On the other hand, they are clearly different from Seyfert 2 galaxies since the ratio of [O III] λ5007 to Hβ is less than 3, i.e., below the limiting value found by Shuder & Osterbrock (1981) to discriminate between Seyfert 1 and Seyfert 2 galaxies. In NLSy1s strong Fe II optical multiplets and higher ionization iron lines (e.g., [Fe VII] λ6087 and [Fe X] λ6375) are often present. These are usually seen in Seyfert 1 and not in Seyfert 2 galaxies.

Many NLSy1s have an unusually strong big blue bump (BBB) which, when compared to typical Seyfert 1 and QSO BBBs, is shifted toward higher energies, sometimes even out of the optical/UV range (at least one object actually peaks in the soft X-ray band: RE J1034+396; Puchnarewicz et al. 1995). Its high-frequency tail is clearly seen in soft X-rays, and these objects have generally steeper soft X-ray continua than is "typical" for Seyfert 1 galaxies (Boller, Brandt, & Fink 1996), meaning that they have a stronger soft X-ray excess over the hard X-ray power law. The intrinsic hard X-ray continua of NLSy1s are also generally steeper (Brandt, Mathur, & Elvis 1997) than in typical Seyfert 1 galaxies. The NLSy1s are usually only weakly absorbed in the soft X-rays (Boller et al. 1996), and in many cases both the UV flux and soft X-ray flux are strongly variable.

NLSy1 objects are generally radio quiet, and their radio powers are typical of those found in other Seyfert galaxies (Ulvestad, Antonucci, & Goodrich 1995).

There is no widely adopted view on the basic reason why the continua of NLSy1 galaxies are different from classical Sy1s. The two most probable explanations of the stronger BBBs in these objects are pole-on orientation (Puchnarewicz, Mason, & Córdova 1994; Wilkes 1999) and higher accretion rate relative to the mass of the central object (e.g., Boller et al. 1996; Wandel 1997; Czerny, Witt, & Życki 1997; Pounds, Done, & Osborne 1995). Steeper hard X-ray spectra and strong permitted Fe II lines are possibly a secondary effect of the atypical shape of the soft X-ray continuum (Pounds et al. 1995; Brandt et al. 1997; Wilkes, Elvis, & McHardy 1987; Shastri et al. 1993).

Wilkes et al. (1999), studying a sample of low-redshift quasars and Sy1s, and their relations between optical/UV emission lines and the continuum, found that the four NLSy1s in their sample show smaller equivalent widths of C III] and C IV lines than typical AGNs [EW(C IV) < 40 Å for NLSy1, while 30 Å < EW(C IV) < 200 Å for other AGNs]. In this paper we investigate in detail the UV-line properties of a sample of NLSy1 objects to determine whether the weakness of the carbon lines is typical of these objects, constituting an additional property that distinguishes them from "normal" Sy1 galaxies. We investigate the physical conditions of the broad-line region (BLR), which may explain these systematic differences. We also discuss the possibility that these objects have luminosities close to their Eddington luminosity.

2. UV-LINE MEASUREMENTS

2.1. *The Sample*

From the currently known set of NLSy1 (Boller et al.

[1] Also Nicolaus Copernicus Astronomical Center, Warsaw, Poland.
[2] Also Harvard-Smithsonian Center for Astrophysics, Cambridge, MA 02138.

1996; Greiner et al. 1996; Puchnarewicz et al. 1992, 1994; Brandt, Fabian, & Pounds 1996; Grupe et al. 1998; Moran, Halpern, & Helfand 1996; W. Brandt 1998, private communication; Wilkes et al. 1999), we have defined a subset of 11 objects (Table 1) for which UV spectra are available either from the *Hubble Space Telescope* (*HST*) (5 objects) or *IUE* archives. The *IUE* spectra were taken from Lanzetta, Turnshek, & Sandoval (1993) and the reduced *HST* spectra from A. Dobrzycki (1998, private communication) (see also Bechtold et al. 2000, in preparation).

2.2. *Line Parameters*

We have measured the EW (Table 2), line ratios (Table 3), and line widths (FWHM; Table 4) of all prominent UV lines: Lyα λ1216, C IV λ1549, C III] λ1909, Si III] λ1892, Al III λ1857, Si IV + O IV] λ1400 blend, and Mg II λ2798.

The EW and FWHM of *IUE* spectra were measured using the SPLOT task in IRAF, the EW by fitting a linear continuum to the data and integrating across the observed emission line (keystroke "e"), the FWHM by measuring the width at half the flux in the line peak above the continuum. The same procedure was applied when the line parameters in the *HST* spectra were measured, although a different program FINDSL (provided by Aldcroft, Bechtold, & Elvis 1994), specially written to handle the *HST* data, was used. The line parameters presented in Tables 2, 3, and 4 have been corrected for absorption: for weak absorption by using a linear fit across the absorption line, for strong absorption (as in PG 1351+560 and PG 1411+442) by assuming a symmetric emission-line profile and reflecting the unabsorbed wing about the peak.

As has been noted by Vestergaard & Wilkes (2000), C III] is blended with Fe III UV34 λ 1914 line, which should be taken into account especially when the C III] line is weak. In three spectra (I Zw1, PG 1211+143, Mrk 478), where the Fe III UV34 was clearly visible, we subtracted this line (modeled as a Gaussian centered at $\lambda = 1914$ Å rest frame) from the C III] blend.

TABLE 1

SAMPLE

Name	α (J2000)	δ (J2000)	z	log νL_ν[a] (2500 Å)
I Zw1[b]	00 53 34.94	+12 41 36.2	0.0611	44.89
E0132−411	01 34 57.36	−40 56 22.4	0.266	45.00
NAB 0205+024	02 07 49.86	+02 42 55.9	0.1564	45.24
PKS 0558−504	05 59 47.37	−50 26 51.8	0.137	45.31
PG 1211+143[b]	12 14 17.60	+14 03 12.5	0.085	45.06
IRAS 13349+2438	13 37 18.73	+24 23 03.3	0.107	45.11
PG 1351+640[c]	13 53 15.78	+63 45 44.8	0.087	44.99
PG 1411+442[b,c]	14 13 48.39	+44 00 13.6	0.090	44.96
Mrk 478[b]	14 42 07.46	+35 26 22.9	0.0781	44.85
PG 1444+407[b]	14 46 45.95	+40 35 06.0	0.267	45.44
II Zw136	21 32 27.81	+10 08 19.5	0.061	45.04

NOTE.—Units of right ascension are hours, minutes, and seconds, and units of declination are degrees, arcminutes, and arcseconds.

[a] The luminosity at 2500 Å has been obtained by extrapolating B (or V) magnitude and assuming a continuum slope of 0.5 ($H_0 = 50$ km s^{-1} Mpc^{-1}).

[b] *HST* spectrum.

[c] Also classified as a broad-absorption line (BAL) QSO.

2.3. *Comparison of NLSy1s with "Normal" AGNs*

In this section we compare the UV-line properties of NLSy1 with Seyfert 1 galaxies and quasars. Figure 1*a* shows the EW of Lyα, C IV, and Mg II of our NLSy1 sample (*shaded areas*) compared to the sample of Seyfert 1 galaxies (*dotted line*) from Wu, Boggess, & Gull (1983) (their sample includes three NLSy1s—I Zw1, Mrk 478, II Zw136—which we excluded here) and low-redshift quasars from Wilkes et al. (1999) and Corbin & Boroson (1996) and radio-loud quasars from Baldwin, Wampler, & Gaskell (1989), combined and denoted by a dashed line. The EW of C IV and Mg II lines are significantly smaller in NLSy1s than in the broad-line Seyfert 1 galaxies and quasars. The Kolmogorov-Smirnov test yielded a 0.001 chance that the EW of C IV and Mg II in NLSy1s and Sy1s are drawn from the same population. For Lyα the chance was less than 0.02. When compared to QSOs the significance remained strong for C IV ($p < 0.01$) and Mg II ($p < 0.025$), while for Lyα the distributions are similar ($p > 0.5$). The smaller EW of the carbon and Mg II lines cannot be due to a simple continuum increase, as this would effect the EW of all lines equally, while EW(Lyα) is not significantly smaller.

TABLE 2

UV-LINE REST-FRAME EW IN Å

	EMISSION LINES							ABSORPTION LINES		
NAME	Lyα	C IV	Si IV + O IV]	Si III]	C III]	Al III	Mg II	Lyα	N V	C IV
I Zw1[a]	171.4	27.9	17.2	9.8	3.3	7.6	25.0	...	1.4	...
0132−411[b]	<140.8	<49.5	...	...	...	...	...	...	...	...
NAB 0205+024	60.9	38.5	...	...	...	...	...	...	0.9	...
PKS 0558−504	32.9	13.7	<5.4	...	...	...	...	...	...	...
PG 1211+143[a]	160.8	49.2	8.4	3.5	4.9	0.0	18.4	...	1.0	...
IRAS 13349+2438[b]	<85.9	...	...	...	...	...	...	...	...	...
PG 1351+640[c]	140.2	>30.0	25.5	...	...	...	12.9	...	<5.2	>2.1
PG 1411+442[a,c]	>79.5	43.6	12.4	5.4	15.8	2.0	18.7	>1.0	14.0	7.5
Mrk 478[a]	123.0[d]	36.0	19.5[d]	9.9	6.6	4.7	...	...	...	...
PG 1444+407[a]	125.5[d]	25.8	22.7	4.6	7.5	4.1	...	...	...	...
II Zw136	110.4	56.6	23.3	...	...	...	32.0	...	...	...

NOTE.—Typical error ~15%.

[a] *HST* spectra.

[b] Low S/N spectrum.

[c] Also classified as a BAL QSO.

[d] Equivalent width obtained from *IUE* spectrum.

TABLE 3

LINE RATIOS

Name	C IV/Lyα	C III]/Lyα	C III]/C IV	Si III]/C III]	Si IV+O IV]/C IV	Si IV+O IV]/Lyα	Mg II/Lyα
I Zw1[a]	0.11	0.01	0.11	2.97	0.85	0.09	0.07
0132−411	>0.21	...	...	...	...	...	...
NAB 0205+024	0.41	...	...	...	...	...	...
PKS 0558−504	0.31	...	...	...	<0.42	<0.13	...
PG 1211+143[a]	0.29	0.03	0.08	0.71	0.18	0.05	0.03
IRAS 13349+2438	...	...	...	...	...	...	...
PG 1351+640[b]	>0.16	...	...	...	0.26	0.04	0.07
PG 1411+442[a,b]	<0.30	<0.13	0.35	0.34	0.30	<0.09	<0.07
Mrk 478[a]	0.24	0.04	0.15	1.5	0.57	0.14	...
PG 1444+407[a]	0.17	0.04	0.22	0.61	0.87	0.15	...
II Zw136	0.34	...	...	...	0.43	0.15	0.01
Observed range	0.11–0.41	0.01–<0.13	0.08–0.35	0.34–2.97	0.18–0.85	0.04–0.15	0.01–0.07
Mean	0.25 ± 0.09[c]	0.05 ± 0.05	0.18 ± 0.11	1.23 ± 1.07	0.49 ± 0.26	0.11 ± 0.04	0.05 ± 0.03
Seyfert 1s observed range[d]	0.35–2.01	0.03–0.39	0.08–0.5	...	...	...	0.07–0.63
Seyfert 1s mean[d]	0.53	...	0.20	...	...	...	0.17
QSOs observed range	0.3–1.04[e]	0.15–0.3[e]	0.46[f]	0.3 ± 0.1[g]	0.3[f]	0.08–0.24[e]	0.15–0.35[e]
LOC maximum reprocessing[h]	0.54	0.28[i]	...	...	0.15	0.08	0.38
LOC integrated[h]	0.57	0.12[i]	...	...	0.11	0.06	0.34

[a] *HST* spectrum.
[b] Also classified as a BAL QSO.
[c] Standard deviation $\sigma = \{[1/(N-1)]\sum_{i=1}^{n}(x_i - \overline{x})^2\}^{1/2}$.
[d] Wu et al. 1983.
[e] Baldwin et al. 1995 and Wilkes et al. 1999.
[f] Composite spectrum from Francis et al. 1991.
[g] Laor et al. 1995.
[h] Line ratios from Baldwin et al. 1995. LOC maximum reprocessing: calculated considering emission from clouds with optimal density and ionizing flux parameters for each line; LOC integrated: calculated integrating over clouds with all possible density and ionizing flux parameters and using the distribution of clouds on the density-flux plane [the assumed dependence with radius and density was $f(r) \propto$ const. and $g(r) \propto n^{-1}$, respectively] as a weighting function.
[i] C III] + Si III] + Al III/Lyα.

As can be seen from Table 3, the C IV/Lyα (mean 0.25 ± 0.09), C III]/Lyα (mean 0.05 ± 0.05), and the Mg II/Lyα (mean 0.05 ± 0.03) ratios are small compared to those typically observed in Seyfert 1 galaxies (Wu et al. 1983 give observed ranges: 0.35–2.01, 0.03–0.39, 0.07–0.63, respectively) and quasars (observed ranges: 0.3–1.04, 0.15–0.3, 0.15–0.35). To show this more clearly, Figure 2 shows the C III]/Lyα versus C IV/Lyα line ratios for NLSy1 in our sample (*filled squares*) with the Seyfert 1 sample (*circles*) and quasars from Laor et al. (1995), Christiani & Vio (1990), and Wilkes et al. (1999) and narrow-line quasars from Baldwin et al. (1988).

As the lines in NLSy1 are narrow, we can clearly resolve the components of the C III] + Si III] + Al III blend (especially

TABLE 4

LINE WIDTHS IN km s^{-1}

Name	Lyα	C IV	Mg II	Hβ[a]
I Zw1[b]	1730	3190	1850	1240
0132−411[a]	<3920	<2460	...	1930
NAB 0205+024	1630	2520	...	1100
PKS 0558−504	3820	3540	...	1500
PG 1211+143[b]	1600	1940	1945	1900
IRAS 13349+2438[c]	<7000	...	...	2100
PG 1351+640[d]	2370	>2110	2140	860
PG 1411+442[b,d]	>1850	2300	1780	2670
Mrk 478[b]	2810	2820	...	1370
PG 1444+407[b]	3700	6180	...	2480
II Zw136	2130	2363	1980	2060
Mean	2960 ± 1611	2942 ± 1237	1939 ± 133	1746 ± 577
QSOs[e]	5399 ± 2757	4793 ± 1765	5566 ± 2426	
QSOs[f]	...	5150 ± 1680	4580 ± 1890	
QSOs[g]	3454 ± 1291	4335 ± 1550	3774 ± 2212	

[a] After Boller et al. 1996.
[b] *HST* spectra.
[c] Very low S/N spectra.
[d] Also classified as a BAL QSO.
[e] Wilkes et al. 1999.
[f] Baldwin et al. 1989.
[g] Corbin & Boroson 1996.

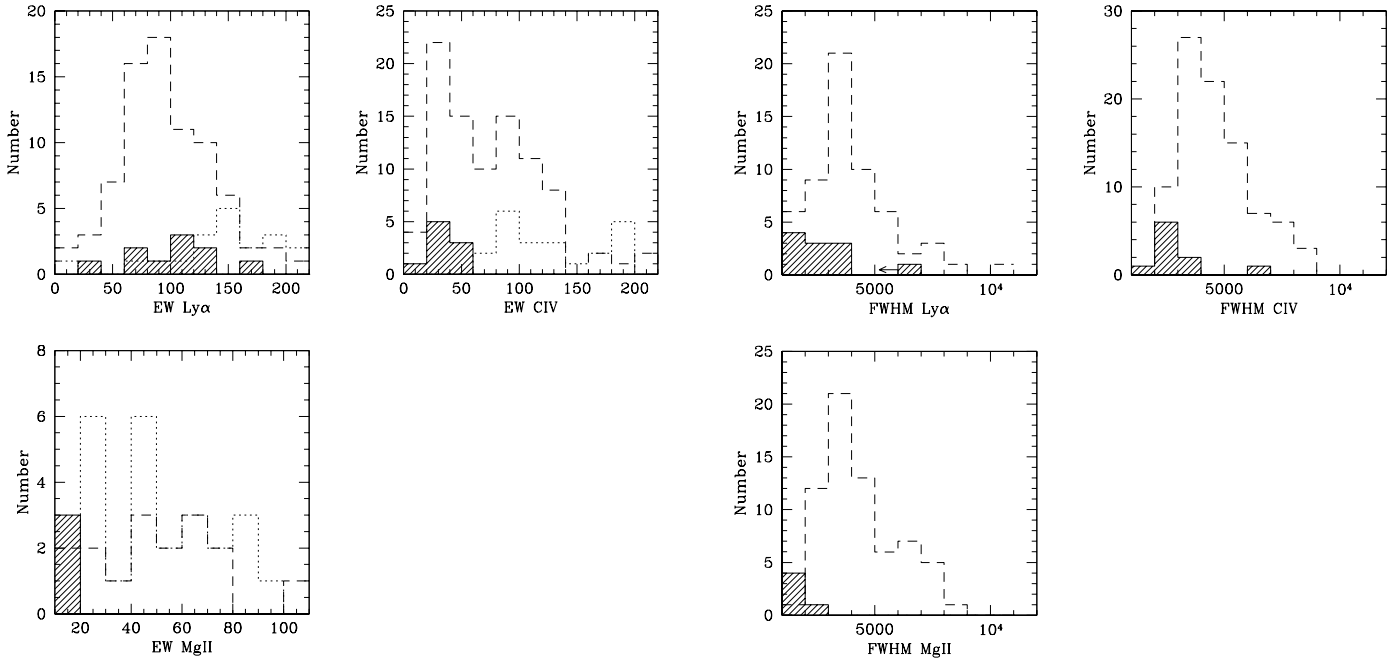

FIG. 1.—(*a*) Comparison of Lyα, C IV, and Mg II equivalent widths in our NLSy1 sample (*shaded areas*) with the Seyfert 1 sample from Wu et al. (1983) (*dotted line*) and QSOs (*dashed line*) from Wilkes et al. (1999), Corbin & Boroson (1996), and Baldwin et al. (1989). (*b*) Comparison of FWHM of Lyα, C IV, and Mg II FWHM, with the same coding as in (*a*).

in the *HST* data; in the *IUE* data the signal-to-noise ratio [S/N] is often too low). From Table 3 it is also clear that the Si III] line in most of the NLSy1 is very strong compared to the C III] line. Also the Si IV+O IV] blend is strong compared to C IV (mean Si IV+O IV]/C IV ratio in NLSy1 is 0.49 ± 0.26, larger than the mean ratio of 0.3 in quasars from Francis et al. 1991). However, the Si IV+O IV]/Lyα ratio is in the range of normal AGNs, indicating that the large Si IV+O IV]/C IV ratio is due to weaker C IV emission. The Al III doublet in NLSy1s is rather strong (equivalent width ~ few Å; see Table 2).

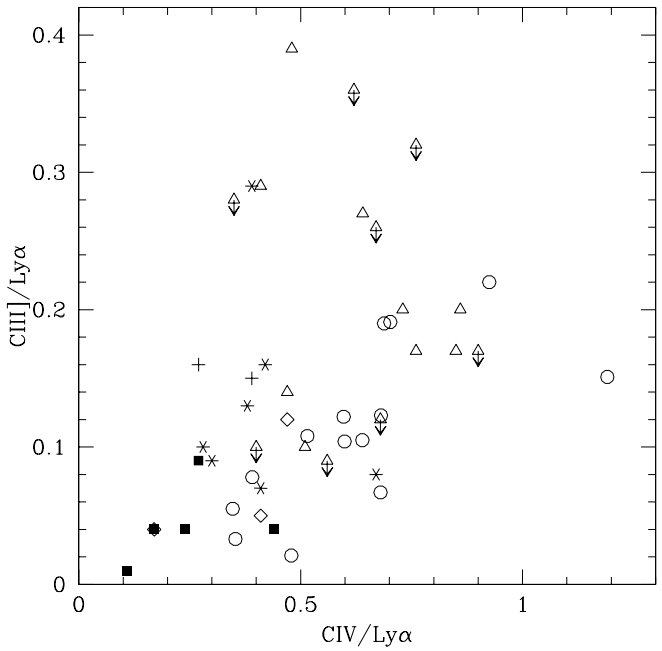

FIG. 2.—Comparison of C III]/Lyα and C IV/Lyα ratios for NLSy1 objects (*filled squares*) and Seyfert 1 galaxies from Wu et al. (1983) (*circles*), QSOs from Laor et al. (1995) (*stars*), Christiani & Vio (1990) (*crosses*), Wilkes et al. (1999) (*triangles*), and narrow-line quasars from Baldwin et al. (1988) (*diamonds*). (For C III] we used the sum of C III]+Si III]+Al III to allow comparison with other samples where the broader lines prevented the authors from separating these components.)

Although broader than Hβ, the UV lines in NLSy1s are narrow compared to other AGNs. In Table 4 and Figure 1*b*, we compare our objects with samples of low-redshift quasars from Corbin & Boroson (1996) and Wilkes et al. (1999) and with a radio-loud sample from Baldwin et al. (1989).

3. DISCUSSION

We will now investigate what the line strengths and line ratios tell us about the physical properties in the BLR clouds of NLSy1s (§ 3.1). Then we will discuss the continuum properties of NLSy1s (§ 3.2) and investigate what they indicate about their central engine. In conclusion, we show how the deduced differences between the central engines of NLSy1s and "normal" AGNs can explain their different, observed emission-line spectra.

3.1. *Physical Properties of the BLR Clouds in NLSy1*

More than ten years ago, Gaskell (1985) noticed that Seyfert 1 galaxies with narrow Hβ lines of FWHM < 1600 km s^{-1} show lower Hβ equivalent widths than typical Seyfert 1 galaxies. He interpreted this finding as a result of collisional destruction of Hβ in the higher density BLR clouds in these objects. Although we do not study the optical spectra of NLSy1s in this paper, we will now investigate whether the UV spectra lead to a similar conclusion.

Rees, Netzer, & Ferland (1989) calculated the line intensities for different BLR cloud densities at constant column density (10^{23} cm^{-2}) and ionization parameter ($U = 10^{-2}$). They found that optically thick lines such as hydrogen and carbon lines have a fairly constant intensity up to a certain density, above which these lines become thermalized and

their intensity drops considerably. For hydrogen lines, C IV, and Mg II, this critical density is $\sim 10^{10}$ cm^{-3}. For the semiforbidden lines C III] and Si III], it is around 5×10^9 cm^{-3} and 10^{11} cm^{-3}, respectively. The Lyα and C IV lines are usually strong coolants at densities smaller than these critical values, but as the density increases and these lines become thermalized, other high-excitation lines such as C III λ977 and Al III λ1857 take over the cooling.

In the previous section we showed that the UV spectra of NLSy1s, when compared to "normal" Seyfert 1 and QSO galaxies, show weaker carbon and Mg II lines. Although the wavelength of our spectra does not cover the range of C III λ977, the Al III λ1857 doublet is clearly seen (where the S/N is high enough) and is especially strong in I Zw1 (see Table 2). All these line properties suggest that in NLSy1 objects the BLR clouds have higher densities than the BLR clouds in "normal" AGNs. We will estimate how much higher by studying the line ratios in the following section.

3.1.1. *The Line Ratios*

The C III]/Lyα and C IV/Lyα ratios are often used as a density indicator. This is because the carbon lines are collisionally excited (hence, sensitive to density), while Lyα is not (note however that Mathur et al. 1994 showed that for large ionizing parameters, $U > 0.1$, where $U = [\int_{1\,\mathrm{Ryd}}^{\infty} (L_\nu/h\nu)d\nu]/(4\pi r^2 c n_{\mathrm{H}})$, C III] ceases to be a density indicator). These line ratios are also a sensitive function of the ionization parameter U, therefore, we investigate the relation of these line ratios to density and U.

We have calculated line ratios using the photoionization code CLOUDY (version 80.07; for reference see Ferland 1991). First, as an input ionizing continuum we took a standard AGN continuum (Table 1 of Mathews & Ferland 1987). With this continuum, the observed lines were only reproduced with higher densities in the C III] than the C IV-emitting clouds. This requires a steep increase in cloud density with radius, which is contrary to expectations and seems unrealistic. Then we used the spectral energy distribution (SED) of the NLSy1 PG 1211+143 as the ionizing continuum. Although no detailed study of the SEDs of NLSy1s has been made and is beyond the scope of this paper, PG 1211+143 is typical of those studied to date with $\alpha_x = 2.13 \pm 0.22$, where $F_\nu = \nu^{-\alpha}$ (Wang, Brinkmann, & Bergeron 1996; where typical NLSy1 slopes are in the range 1.5–3.5; see Boller et al. 1996) and $\alpha_{io} = 0.90$ (i.e., slope measured between 1 μm and 2500 Å, where typical NLSy1 values are 0.4–2.8; see Lawrence et al. 1997). The IR to hard X-ray SED of this object was taken from Elvis et al. (1994) and is reproduced here in Figure 3. The SED was linearly interpolated between the observational points in the optical/UV region. The EUV continuum was determined by a linear interpolation between the lowest energy point in the X-ray range and the highest in the UV, providing a conservative (i.e., low) estimate of the number of EUV photons. We investigated a range of cloud densities [n(H) = 10^8–10^{13} cm^{-3}, well within the range of the applicability of the photoionization code CLOUDY[3]] and ionization parameters ($U = 10^{-3}$ to 10^{-1}, where $U = 10^{-2}$ is the value for the "standard" BLR; Davidson & Netzer 1979). The metal abundances were assumed to be solar and the cloud column density 10^{23} cm^{-2}. The calculated line ratios are plotted in Figure 4, where the observed line ratios for our NLSy1 are denoted by horizontal lines. The C IV/Lyα ratio (Fig. 4*a*) depends very strongly (more than any other line ratio) on the value of the ionization parameter as well as on the density of the BLR clouds. Small values of the ionization parameter ($U = 10^{-3}$) are clearly favored by our data, for which densities of the order of 10^{11}–10^{12} cm^{-3} are needed to produce the low observed C IV/Lyα ratios. For the same small ionization parameter, the observed C III]/Lyα ratios indicate densities between 10^9 and 10^{11} cm^{-3} (see Fig. 4*b*), which are smaller than the cloud densities inferred from the C IV/Lyα ratios. This strongly suggests that the C III] and C IV lines are formed in different clouds, which implies a stratified BLR. This is as expected from the results of reverberation mapping (e.g., NGC 5548: Korista et al. 1995; NGC 7469: Wanders et al. 1997; Fairall 9: Rodriguez-Pascual et al. 1997), which show that the C IV and Lyα line fluxes vary with a smaller time delay, relative to the UV continuum, than the C III] lines, indicating that C IV, Lyα–emitting clouds lie nearer to the central engine than the C III]-emitting clouds. The density of the C IV- and Lyα-emitting line region is typically estimated (e.g., Peterson et al. 1985) to be $\sim 10^{11}$ cm^{-3}, while the C III] region is $\sim 10^{9.5}$ cm^{-3}. Thus, the density of the C IV, Lyα–emitting clouds in our NLSy1s is comparable or somewhat (<10 times) larger than in normal AGNs.

To further constrain the density of the C III]-emitting clouds, we need to investigate its ratio to a line that is

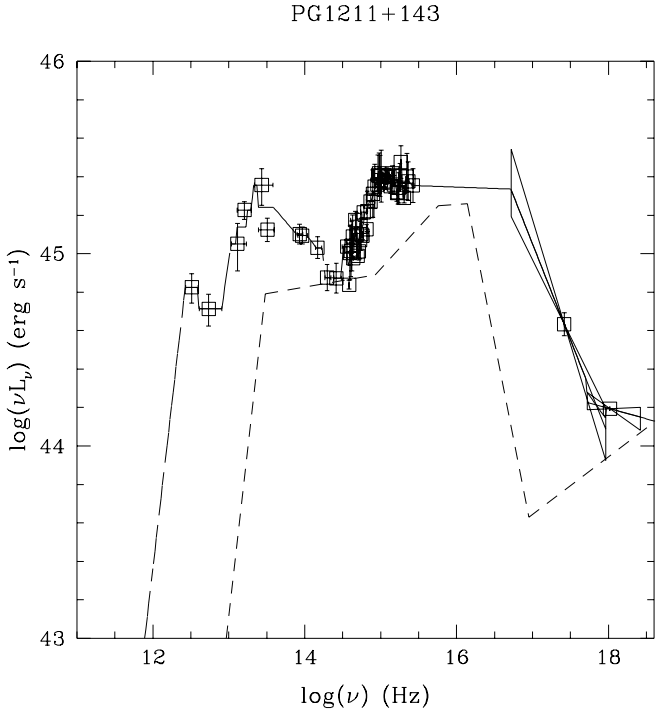

FIG. 3.—IR to hard X-ray spectral energy distribution of PG 1211+143 (from Elvis et al. 1994), which was used as an input ionizing continuum in the photoionization calculations. The dotted line indicates the standard AGN continuum of Mathews & Ferland (1987) used in CLOUDY normalized at 1 μm. The NLSy1s have a more pronounced BBB and a strong soft X-ray excess.

[3] "The hydrogen and atoms and ions of helium are treated in the code as 10-level atoms. The treatment of the heavy elements is not as complete as hydrogen and helium, but a 3-body recombination is included as a general recombination process. [...] The physical high-density limit is set by the approximate treatment of the three-body recombination-collisional ionization ($\lesssim 10^{13}$ cm^{-3}) for the heavy elements and the approximate treatment of line transfer" (see Ferland 1991).

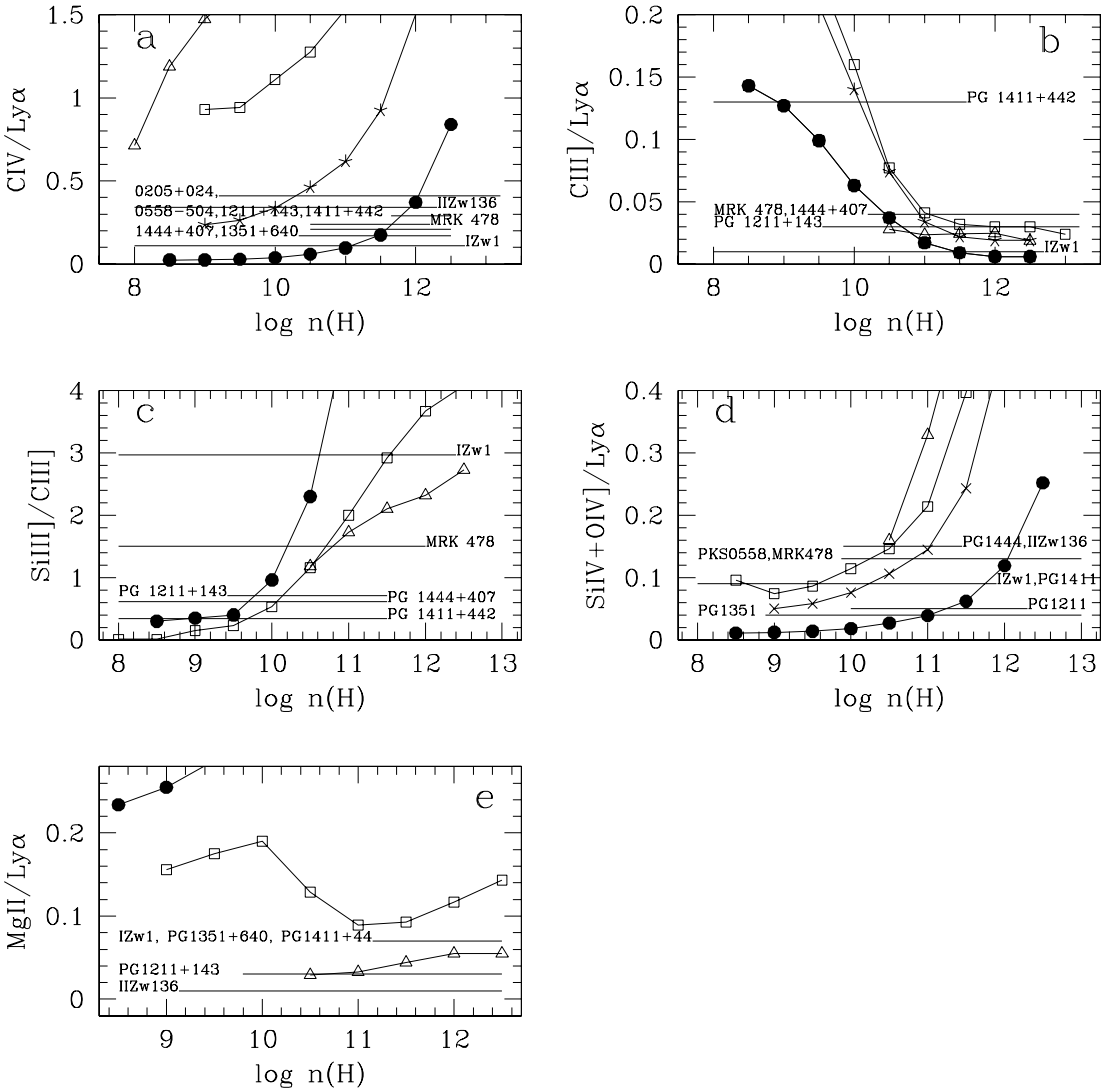

FIG. 4.—Calculated line ratios of (*a*) C IV/Lyα, (*b*) C III]/Lyα, (*c*) Si III]/C III], (*d*) Si IV + O IV]/Lyα, (*e*) Mg II/Lyα, for several different ionization parameters. Triangles denote log $U = -1$, squares log $U = -2$, filled circles log $U = -3$, and stars log $U = -2.5$. Horizontal lines show the observed line ratios.

formed in the same clouds, for example, Si III]. For $U = 10^{-3}$ the density of the emitting gas inferred from the Si III]/C III] line ratio is between $10^{9.5}$ and $10^{10.5}$ cm^{-3} (see Fig. 4*c*; we omit here PG 1411+442, which is a broad absorption line QSO and has n(H) $\sim 10^9$ cm^{-3}). The ratio of Si III]/C III] is larger than the typical value of $\sim 0.3 \pm 0.1$ seen in quasars (Laor et al. 1995) for all objects (except for BAL QSO PG 1411+442; see Table 3 and Fig. 4*c*) This high ratio is probably the result of the suppression of C III] while Si III] remains strong due to the smaller critical density for C III] ($\geq 5 \times 10^9$; cf. 10^{11} cm^{-3} for Si III]; see § 3.1).

In Figure 4*d* we present the observed and calculated Si IV + O IV]/Lyα ratios. For $U = 10^{-3}$ the clouds have density of the order of 10^{11}–10^{12} cm^{-3}, similar to the range for C IV- and Lyα-emitting clouds.

The Mg II/Lyα ratio, on the other hand, is very small and cannot be reproduced by clouds with small ionization parameters even when the column density, $N_{\rm H}$, is varied over the range 10^{22}–10^{24} cm^{-2}. Only larger than standard ionization parameters, in the range 10^{-1} to 10^{-2}, can produce the observed ratios (Fig. 4*e*). This may indicate that the Mg II lines do not form in the same region as the other BLR lines. We will return to this problem in the next section.

To summarize the results of this subsection, we conclude that the unusual UV-line ratios in the NLSy1 objects can be explained if the BLR clouds have 10 times lower ionizing parameters (log $U \sim -3$) and a few times (<10) higher densities (n(H) $\sim 10^{11}$–10^{12} cm^{-3} for Lyα-, C IV-, Si IV-emitting clouds and $10^{9.5}$–$10^{10.5}$ cm^{-3} for C III]-, Si III]-emitting clouds) than normal AGNs. The BLR is clearly stratified with C IV, Lyα, Si IV producing clouds lying closer to the central engine, while C III] and Si III]-emitting clouds lie predominantly farther out. The Mg II emission cannot be produced by the same cloud population, suggesting that these lines form in a different region.

Although clouds with a wide range of properties are likely to exist in the broad-line region, it was shown by Baldwin et al. (1995) and Korista et al. (1997) that each emission line is most efficiently produced in gas with the optimum parameters for that line. These are the so-called locally optimally emitting clouds or LOCs. Thus, our modeling derives the parameters of the LOCs for each line so that the line fluxes and ratios provide a good approx-

imation to a detailed multizone model of the BLR (see Baldwin et al. 1995; Korista et al. 1997; and our Table 3), which is beyond the scope of this paper.

3.1.2. *The Weak* Mg II *Problem*

The Mg II line is surrounded on both sides by Fe II emission. As the Fe II emission in NLSy1s is usually very strong (Boller et al. 1996), it is possible that the wings of Mg II disappear in the stronger iron bumps. This effect could lead to an underestimation of the Mg II emission of up to a factor of 2 in the strongest Fe II sources (such as I Zw1; see Vestergaard & Wilkes 2000). However, even if our measurements were underestimating the Mg II emission by such a large factor, the real Mg II/Lyα ratio would still be much smaller than that observed in quasars or in the lower end of the range for Seyfert 1 galaxies (see Table 3). The ionization parameter U inferred from the observed line ratio would be $\sim 10^{-1}$ to 10^{-2} (see Fig. 4*e*), still larger than that inferred from the other emission lines.

Thus, we conclude that the Mg II-emitting clouds have a different value of the ionization parameter and are formed in a physically different region of the BLR (consistent with the different time lags shown by Lyα, C IV, and Mg II lines in NGC 5548). Photoionization models predict that Mg II is either formed in a partially ionized zone (PIZ) of the BLR clouds or in a low-ionization region (LIL) separate from the high-ionization region (HIL) where the Lyα, C IV, C III] lines are formed (Collin-Souffrin et al. 1988). If the Mg II line is formed in a PIZ, it is possible that the stronger BBB in NLSy1s will push the ionization front farther back into the cloud, resulting in a smaller PIZ and weaker Mg II emission than for objects with a "normal" BBB.

However, the weaker Mg II emission is not consistent with the stronger Fe II optical emission observed in NLSy1s, which in photoionization models is predicted to be formed in the same region (PIZ: Krolik & Kallman 1988; LIL: Collin-Souffrin et al. 1988). This inconsistency suggests that the Fe II emission is instead generated in a different region from Mg II. The observations of line variability in NGC 5548 (Sergeev et al. 1997) showed that the Fe II optical multiplets have a very long time lag of several hundred days, while the Mg II has a 30–50 day time lag, also implying that these lines are formed in different regions. The Fe II lines may be produced in the outer regions of the accretion disk as suggested by Dumont & Collin-Souffrin (1988) or in a separate, mechanically heated region closely related to the compact radio source (hence, the observed anticorrelation of Fe II emission and radio flux).

3.2. *High Luminosity to the Eddington Luminosity Ratio*

It has been suggested by a number of authors that NLSy1 galaxies as a class have systematically higher ratios of their luminosity to the Eddington luminosity, i.e., they have systematically lower masses in a given luminosity range than Sy1 galaxies and QSOs (Pounds et al. 1995; Wandel 1997). This suggestion was made based on the analogy with the Galactic black hole candidates. We will address this suggestion now.

3.2.1. *Continuum Properties*

One of the current explanations of the soft X-ray excess in AGNs is reprocessing of the hard X-rays by partially ionized, optically thick matter, probably in the accretion disk. The model describes well the soft X-ray continuum of low-luminosity, flat $\alpha_{\rm softX}$ Seyfert galaxies but has problems with fitting the steepest $\alpha_{\rm softX}$ spectra (see Fiore, Matt, & Nicastro 1997), which characterize NLSy1. The steep $\alpha_{\rm softX}$ can instead be explained by emission from the innermost part of an accretion disk which is then Comptonized by an optically thin, hot corona surrounding the disk (Czerny & Elvis 1987; Laor et al. 1997).

Theoretical models that can explain both the presence of the BBB and the hard X-ray emission are based either on radial or horizontal stratification between the hot, optically thin and cold, optically thick accretion flow (Wandel & Urry 1991; Shapiro, Lightman, & Eardley 1976; for a review see Wandel & Liang 1991). In this paper we use the model of an accretion disk corona (ADC) by Witt, Czerny, & Życki (1997), where the corona itself accretes and generates energy through viscosity, and the division of the flow into optically thin and optically thick regions results from the cooling instability discussed by Krolik, McKee, & Tarter (1981). Such a model is able to predict the fraction of the energy generated in the corona instead of adopting this quantity as a free parameter. The model is fully defined by three parameters: the mass of the central black hole ($M_{\rm bh}$), the accretion rate or the ratio of the luminosity to the Eddington luminosity ($L/L_{\rm Edd}$), and the viscosity parameter ($\alpha_{\rm vis}$, assumed to be the same in both the disk and the corona). The model predicts a systematic change in the optical/UV/X-ray spectral energy distribution due to a change in $L/L_{\rm Edd}$. A larger ratio results in a more pronounced BBB, which is shifted toward higher energies (resulting in stronger soft X-ray emission and hence steeper soft X-ray slopes).

We have determined continuum properties predicted by this model over a large range of $L/L_{\rm Edd}$ (0.001–0.7), $\alpha_{\rm vis}$ (0.02–0.4), and black hole masses (10^6–10^{10} $M_\odot$). We then compared the observed continua of our NLSy1s with the UV luminosity at 2500 Å and the soft and hard X-ray slopes ($\alpha_{\rm softX}$ and $\alpha_{\rm hardX}$) predicted by the model. Table 5 shows the observed $\alpha_{\rm softX}$ (from *ROSAT*) and $\alpha_{\rm hardX}$ (from *ASCA*) slopes for each object, while Table 6 gives the best-fitted model parameters for each object. Our model was able to reproduce the steep soft and hard X-ray slopes within the observed uncertainties for most of the NLSy1s. However, for two objects (I Zw1, PKS 0558−504) we did not succeed in fitting both the soft and hard X-ray slopes simultaneously. This may be due to the way we treat Comptonization in our model (see Janiuk & Czerny 2000 for further details). In Figures 5*a* and 5*b* we show how the X-ray slopes change with the model parameters. Each curve represents one value of $L/L_{\rm Edd}$ and $\alpha_{\rm vis}$ and a full range of black hole masses, where smaller $M_{\rm bh}$ lie at smaller 2500 Å luminosities. We see clearly that only the large ratios of $L/L_{\rm Edd}$ can give the steep, observed soft X-ray slopes.

As has been shown by Czerny et al. (1997), quasars radiate usually at $\sim$0.01–0.2 of their Eddington luminosity, while Seyfert galaxies radiate at $\sim$0.001–0.3. Our NLSy1s (where we use the same ADC model as Czerny et al. 1997 to fit the parameters of the central engine) radiate at $L/L_{\rm Edd} \sim$ 0.27–0.58, much larger than the typical AGN. The masses of the central black hole calculated from the model ($\sim 10^8$–10^9 $M_\odot$) for our objects are of the same order as masses found in typical Seyfert 1 galaxies, but the bolometric luminosities are larger and comparable to those of QSOs (see Wilkes et al. 1999, Table 12 for comparison). This is deduced from the stronger, higher energy BBB and places the NLSy1 in a

TABLE 5

OBSERVED SOFT AND HARD X-RAY INDICES

Name	α (0.1–2.5 keV)	Reference	α (2–10 keV)	Reference
I Zw1	2.0 ± 0.1	1	1.3 ± 0.06	7
0132−411	3.1 ± 0.6	1	...	
NAB 0205+024	2.8 ± 0.5	2	1.09 ± 0.10	10
PKS 0558−504	1.9 ± 0.1	3	1.26 ± 0.05	3
PG 1211+143	2.13 ± 0.22	4	1.01 ± 0.06	8
IRAS 13349+2438	1.70 ± 0.33	5	$1.22^{+0.08}_{-0.08}$	8
PG 1351+640[a]	1.53 ± 0.63	4	...	
PG 1411+442[a]	1.97 ± 0.46	4	...	
Mrk 478	2.6 ± 0.1	1	0.95 ± 0.13	8
PG 1444+407	2.2 ± 0.3	1	...	
II Zw136	$1.25 \pm$ ...	6	1.17 ± 0.07[b]	9

[a] Also classified as a BAL QSO.

[b] Slope from *Ginga* determined between 2 and 18 keV (reference 9).

REFERENCES.—(1) Boller et al. 1996; (2) Fiore et al. 1995; (3) W. Brandt 1998, private communication; (4) Wang et al. 1996; (5) Brandt et al. 1996; (6) Wang, Lu, & Zhou 1998 (error on α [0.1–2.5 keV] not available); (7) Hayashida 1997; (8) Brandt et al. 1997; (9) Lawson & Turner 1997; (10) Fiore et al. 1998.

transition zone between the Sy1s and QSOs, i.e., among Sy1s with larger luminosities or QSOs with lower masses. We note that, while the absolute numbers we deduce depend upon the particular ADC model used, the general trends do not.

3.2.2. *Density and the Radius of the BLR*

The structure and the dynamics of the BLR are complex, as suggested by variability studies in the case of Seyfert galaxies. However, we can analyze the scaling properties of the whole BLR of an object with the properties of the central source, including the shape of the X-ray continuum.

The BLR gas Compton heated by the ionizing continuum will form (in any geometry) two phases: a cool phase with $T_c \sim 10^4$ (the BLR clouds) and a hot phase with $T_h \sim 10^8$ (the intercloud medium; see Krolik & Kallman 1988; Czerny & Dumont 1998; Wandel & Liang 1991), when in equilibrium. The precise values of these temperatures depend on the shape of the continuum.

In the context of the two-phase model, we will now investigate how the properties of the BLR change due to the steeper X-ray continuum of an NLSy1. We use the ionization parameter of Krolik et al. (1981):

$$\Xi = \frac{2.3F_{\rm ion}}{cp} = \frac{2.3F_{\rm ion}}{ck\rho_c T_c/\mu H}\,, \tag{1}$$

where p is the total pressure, ρ_c and T_c are the density and temperature of the cold phase, and $F_{\rm ion}$ is the flux above 1 ryd determined by the ionizing luminosity of the central source $L_{\rm ion}$ and the current radius r (where effects of geometry have been neglected):

$$F_{\rm ion} = L_{\rm ion}/4\pi r^2\,. \tag{2}$$

The two phases coexist at a value of the ionization parameter, Ξ_h, that scales with the hot phase temperature, T_h in the following way (Begelman, McKee, & Shields 1983):

$$\Xi_h = 0.65\left(\frac{T_h}{10^8}\right)^{-3/2}\,. \tag{3}$$

TABLE 6

SOFT AND HARD X-RAY INDICES FROM BEST-FIT MODEL

Name	$L/L_{\rm Edd}$	$\alpha_{\rm vis}$	log $M_{\rm bh}$	$\alpha_{\rm softX}$[a]	$\alpha_{\rm hardX}$[b]
I Zw1[c]	0.58	0.027	7.93	2.02	1.17
0132−411[d]	0.27	0.30	8.29	2.52	1.05
NAB 0205+024	0.27	0.30	8.45	2.50	1.04
PKS 0558−504[c]	0.58	0.027	8.89	1.89	1.14
PG 1211+143	0.30	0.14	8.26	2.02	1.05
IRAS 13349+2438	0.58	0.03	8.12	1.99	1.15
PG 1351+640[d,e]	0.27	0.03	8.20	1.51	1.11
PG 1411+442[d,e]	0.58	0.027	7.96	2.00	1.17
Mrk 478	0.27	0.3	8.12	2.53	1.07
PG 1444+407[d]	0.27	0.3	8.61	2.49	1.04
II Zw136	0.27	0.03	8.20	1.51	1.11

[a] Soft X-ray index measured from 0.1 to 2.5 keV corresponding to a *ROSAT* slope.

[b] Hard X-ray index measured from 2 to 10 keV corresponding to an *ASCA* slope.

[c] We could not fit both the soft and hard X-ray slopes simultaneously.

[d] These objects do not have observed hard X-ray slopes, hence, the derived model parameters are not well constrained.

[e] Also classified as a BAL QSO.

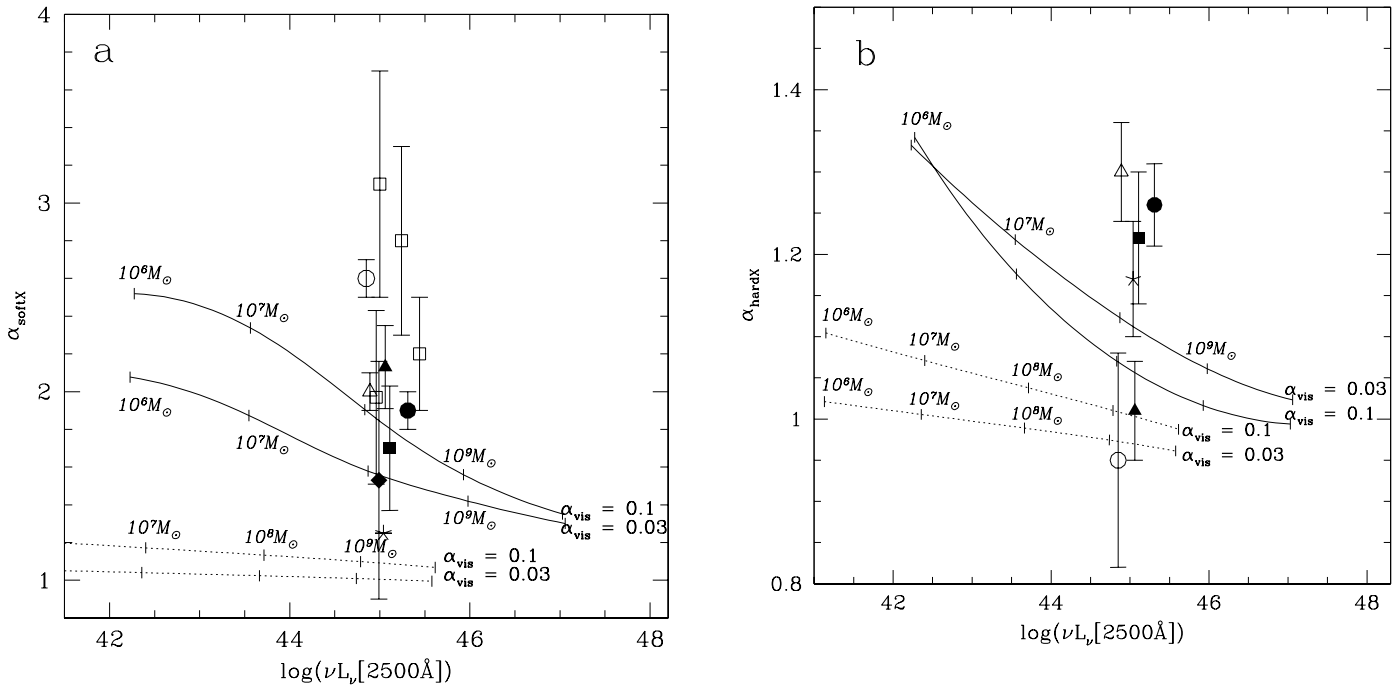

FIG. 5.—Comparison of the (*a*) soft and (*b*) hard X-ray spectral slopes of NLSy1 objects in our sample with those predicted by the ADC model. Each curve represents one value of L/L_{Edd} and α_{vis} with varying black hole masses as labeled (smaller M_{bh} lie at the smaller 2500 Å luminosities). Dashed lines denote small $L/L_{Edd} = 0.01$, solid line $L/L_{Edd} = 0.3$. The value of viscosity parameters are as labeled. Clearly, the larger L/L_{Edd} are needed to reproduce the steep soft X-ray slopes of NLSy1s. *Open triangle*: I Zw1; *filled circle*: PKS 0558−504; *filled triangle*: PG 1211+143; *filled square*: IRAS 13349+248; *filled diamond*: PG 1351+640; *open circle*: Mrk 478; *star*: II Zw136.

The BLR is most probably radially extended. For the purpose of exploring the various dependencies, we determine a representative radius for the BLR. Note that this is a scaling factor rather than the specific radius at which a particular emission line is generated. If the cloud number density profile is flatter than r^{-2}, then most of the emission would come from the outer radii of the BLR. As in the case of the inverse Compton–heated coronae discussed by Begelman et al. (1983), a nearly hydrostatic corona will exist up to a radius where the temperature of the hot medium is equal to the "escape" temperature (i.e., the virial temperature). At larger radii the corona is heated to temperatures exceeding the escape temperature, becomes unstable, and forms an outflowing wind. We therefore identify the outer edge of the BLR, r_{BLR}, with the radius where the hot medium temperature is equal to the virial temperature

$$kT_h = \frac{GM_{bh} m_H}{r_{BLR}} . \quad (4)$$

The size of the BLR expressed in units of the Schwarzschild radius, R_{Schw}, is then given by

$$r_{BLR}/R_{Schw} = \frac{m_H c^2}{2kT_h} , \quad (5)$$

so a lower value of the hot medium temperature in NLSy1 galaxies is consistent with larger values of r_{BLR}/R_{Schw} and, consequently, lower values of the typical velocities.

A similar conclusion, that the BLR radius is larger in NLSy1s, was reached by Wandel (1997), who assumed that the representative radius of the BLR is determined by the requirement to have a standard value of the ionization parameter. He then showed that the size of the BLR region is dependent not only on the luminosity of the central source but also on the soft X-ray spectral slope. A steeper (softer) X-ray spectrum has a stronger ionizing power, and hence, for a constant ionizing parameter, the BLR clouds are at larger distances from the central source, have smaller velocity dispersions, and as a result form narrower emission lines. Laor et al. (1995) also reach a similar conclusion, but in their picture the narrow lines in NLSy1s result purely from the lower black hole mass. In our scenario the lower black hole mass and the shape of the SED (i.e., the steeper soft X-rays that decrease T_h) combine to produce the narrow lines.

Combining equations (1)–(4), we estimate the cloud density,

$$\rho_c \sim \frac{L}{M_{bh}^2} \times \frac{T_h^{7/2}}{T_c} , \quad (6)$$

or using logarithms,

$$\log \rho_c \sim \log L - 2 \log M_{bh} + 7/2 \log T_h - \log T_c . \quad (7)$$

As has been argued in § 3.2.1, NLSy1s have bolometric luminosities comparable to QSOs, although their central black holes have lower masses. The median value of a black hole in quasars is $\sim 10^{10}\ M_\odot$ (see Czerny et al. 1997 calculations), while the median black hole mass in NLSy1s (as inferred from our calculations, using the same ADC model; see Table 6) is $10^{8.26}\ M_\odot$, i.e., ~ 55 times lower. Let us assume that a typical quasar SED is composed of a power law and an accretion disk spectrum peaking at 10 eV

(log ν = 15.38, 1240 Å), while a typical NLSy1 SED has a power law and a disk peaking at 80 eV (however, note that the most extreme NLSy1, RE J1034+396, has its peak at 120 eV; see Puchnarewicz et al. 1995). Krolik & Kallman (1988) calculated the Compton temperatures of the hot phase for these SEDs, normalizing both to have the same total ionizing energy. The 10 eV bump spectrum gave Compton temperatures $\sim 3.0 \times 10^7$ K, while the 80 eV bump gave a lower temperature $\sim 8.0 \times 10^6$ K. At the same time the temperature of the cool phase increased by a factor of $\sim$3.0 (0.5 in logarithm; see Fig. 2 of Krolik & Kallman 1988). Hence, the Compton temperature of the hot phase in NLSy1s and QSOs differs by $\log T_{h,\mathrm{NLSy1}} - \log T_{h,\mathrm{QSO}} = -0.57$, and the temperature of the cold phase is larger by $\log T_{c,\mathrm{NLSy1}} - \log T_{c,\mathrm{QSO}} = 0.5$. Substituting the above values into equation (7) implies that $\log \rho_{c,\mathrm{NLSy1}} - \log \rho_{c,\mathrm{QSO}} \approx 1$, i.e., the densities of the BLR should be higher by a factor of 10 in NLSy1 than in typical QSOs with redder BBB.

The larger BLR radii and larger by a factor 10 densities obtained from our modeling (as being due to hotter BBBs) are consistent with the narrow lines and line ratios observed in NLSy1s. Thus, we conclude that the unusually hot and strong BBB in NLSy1s can naturally produce their observed UV spectra.

4. NLSy1 VERSUS BAL QSOs

It has been suggested (e.g., Leighly et al. 1997; Lawrence et al. 1997) that there may exist a connection between NLSy1s and BAL QSOs. Both these classes have strong Fe II λ4570 and Al III λ1857 emission and weak C IV λ1549 and [O III] λ5007. Their continua are red in the optical and strong in the IR; additionally, both classes are mostly radio quiet. Leighly et al. (1997) reported evidence for relativistic outflows in three NLSy1s.

Observationally, there are also many differences. NLSy1s are strong soft X-ray emitters, while BAL QSOs are weak, possibly due to X-ray absorption (Mathur, Elvis, & Singh 1995). BAL QSOs are thought to be seen more edge-on, at viewing angles skimming the edge of the dusty torus (Turnshek et al. 1996; Aldcroft, Elvis, & Bechtold 1993). NLSy1s, on the other hand, are probably viewed more face-on, as they show low absorption from the torus (Boller et al. 1996), and some even show beaming in their radio spectra (e.g., PKS 0558−504; Remillard et al. 1991).

In high-resolution *HST* spectra, NLSy1s show absorption features that are much weaker than in BAL QSOs (see Table 2). However, this is expected since 50% of Seyfert 1 galaxies show absorption features (Crenshaw 1995). The optical spectra of some BAL QSOs may resemble the spectra of NLSy1s, showing narrow Hβ with FWHM < 2000 km s^{-1} (that is why the two BAL QSOs, PG 1351+640 and PG 1411+442, were initially chosen to be in our sample), but this only cautions us that basing classifications on optical spectra alone is potentially misleading.

5. CONCLUSIONS

In this paper we have studied the UV emission-line properties of a class of extreme optical/UV/X-ray AGNs: the narrow-line Seyfert 1 galaxies. We found 11 NLSy1s that had been observed in the UV by either *HST* or *IUE*. We have shown that in comparison with "normal" broader line AGNs the equivalent widths of C IV and Mg II are significantly smaller [NLSy1s have EW(C IV) < 60 and EW(Mg II) < 20; normal AGNs have EW(C IV) < 210 and EW(Mg II) < 120], the EW of Al III is larger (few Å), and the UV line widths are narrower (although not as narrow as the optical Hβ line). Also, the C III]/Lyα, C IV/Lyα, and Mg II/Lyα line ratios are smaller, while those of Si III]/C III], Si IV+O IV]/C IV lines are larger. Photoionization models predict that these line ratios are formed in material with densities higher, by a factor of a few (< 10) than standard BLR cloud densities and with the ionization parameter lower by a factor of 10. These parameters, however, predict higher Mg II/Lyα ratio, in contradiction to the lower ratios observed requiring that Mg II be produced in a separate region.

We have fitted the SEDs of our NLSy1s to the Witt et al. (1997) model of an accretion disk with a Compton-cooled corona and found that NLSy1s radiate at $0.27 < L/L_{\mathrm{Edd}} < 0.58$, much larger than the typical AGN ($L/L_{\mathrm{Edd}} < 0.3$). The masses of the central black holes calculated from the model are, in our objects, of the order of masses found in typical Seyfert 1 galaxies ($10^8\ M_\odot$), but the bolometric luminosities ($\nu L_\nu \sim 10^{46}$ ergs s^{-1}) are larger and comparable to those of QSOs.

Krolik & Kallman (1988) predict that steeper soft X-ray BBBs, such as these of NLSy1s, change the equilibrium of the two-phase cloud-intercloud medium, decreasing the temperature of the hot intercloud medium (which we assume to be the corona above the accretion disk) and increasing the temperature of the cool BLR clouds. We show that this change in equilibrium increases the density of the BLR clouds, resulting in a change of the observed line intensities and ratios consistent with these in NLSy1s. In addition, the resulting decrease in T_h causes an increase in the radius of the BLR, a correspondingly lower velocity dispersion, and narrower lines as observed in NLSy1s.

The NLSy1s lie at the extreme end of the Boroson & Green eigenvector 1 (Boroson & Green 1992), which was then found (Brandt & Boller 1998) to link the soft X-ray properties with the optical properties, i.e., the Fe II/Hβ and [O III] strengths and Hβ line width. We have found that the NLSy1s have very weak C IV and C III] lines and narrow UV lines extending the set of parameters linked to eigenvector 1. The large BLR cloud densities, deduced from these characteristic UV-line ratios, are probably due to the steep soft X-ray SEDs, which are in turn the result of larger L/L_{Edd} ratios (as inferred from the Witt et al. 1997 ADC model). In this scenario a larger L/L_{Edd} is the physical parameter driving the Boroson & Green eigenvector 1.

We are grateful to Niel Brandt for helping us to obtain a complete list of known NLSy1s and their X-ray slopes, Adam Dobrzycki for providing us with the *HST* data, and Ken Lanzetta for the *IUE* Atlas of AGN spectra. We wish to thank Martin Gaskell, Martin Elvis, Marianne Vestergaard, Kirk Korista, and Suzy Collin-Souffrin for valuable discussions and thank the anonymous referee for comments that improved the manuscript. J. K. gratefully acknowledges the support of a Smithsonian predoctoral fellowship at the Harvard-Smithsonian Center for Astrophysics and grant 2P03D018.16 of the Polish State Committee for Scientific Research (J. K. and B. Cz.). B. J. W. acknowledges NASA contract NAS 8-39073 (Chandra X-Ray Center) and S. M. a NASA grant NAG 5-3249 (LTSA).

REFERENCES

Aldcroft, T., Bechtold, J., & Elvis, M. 1994, ApJS, 93, 1
Aldcroft, T., Elvis, M., & Bechtold, J. 1993, AJ, 105, 2054
Baldwin, J. A., Ferland, G., Korista, K., & Verner, D. 1995, ApJ, 455, L119
Baldwin, J. A., McMahon, R., Hazard, C., & Williams, R. E. 1988, ApJ, 327, 103
Baldwin, J. A., Wampler, E. J., & Gaskell, S. M. 1989, ApJ, 338, 630
Begelman, M. C., McKee, C. F., & Shields, G. A. 1983, ApJ, 271, 70
Boller, Th., Brandt, W. N., & Fink, H. 1996, A&A, 305, 53
Boroson, T. A., & Green, R. F. 1992, ApJS, 80, 109
Brandt, W. N., & Boller, Th. 1998, Astron. Nachr., 319, 163
Brandt, W. N., Fabian, A. C., & Pounds, K. A. 1996, MNRAS, 278, 326
Brandt, W. N., Mathur, S., & Elvis, M. 1997, MNRAS, 285, L25
Christiani, S., & Vio, R. 1990, A&A, 227, 385
Collin-Souffrin, S., Dyson, J. E., McDowell, J. C., & Perry, J. J. 1988, MNRAS, 232, 539
Corbin, M. R., & Boroson, T. A. 1996, ApJS, 107, 69
Crenshaw, D. M. 1995, BAAS, 187, 24.05
Czerny, B., & Dumont, A.-M. 1998, A&A, 338, 386
Czerny, B., & Elvis, M. 1987, ApJ, 321, 305
Czerny, B., Witt, H. J., & Życki, P. T. 1997, in Proc. Second INTEGRAL Workshop (ESA SP-382; Noordwijk: ESA), 397
Davidson, K., & Netzer, H. 1979, Rev. Mod. Phys., 51, 715
Dumont, A. M., & Collin-Souffrin, S. 1990, A&A, 229, 313
Elvis, M., et al. 1994, ApJS, 95, 1
Ferland, G. F. 1991, HAZY, OSU Astronomy Department Internal Report
Fiore, F., Elvis, M., Siemiginowska, A., Wilkes, B. J., McDowell, J. C., & Mathur, S. 1995, ApJ, 449, 74
Fiore, F., et al. 1998, MNRAS, 298, 103
Fiore, F., Matt, G., & Nicastro, F. 1997, MNRAS, 284, 731
Francis, P. J., Hewett, P. C., Foltz, C. B., Chaffee, F. H., Weymann, R. J., & Morris, S. L. 1991, ApJ, 373, 465
Gaskell, C. M. 1985, ApJ, 291, 112
Greiner, J., Danner, R., Bade, N., Richter, G. A., Kroll, P., & Komossa, S. 1996, A&A, 310, 384
Grupe, D., Beuermann, K., Thomas, H.-C., Mannheim, K., & Fink, H. H. 1998, A&A, 330, 25
Hayashida, K. 1997, in Emission Lines in Active Galaxies: New Methods and Techniques, ed. B. M. Peterson, F.-Z. Cheng, & A. S. Wilson (San Francisco: ASP), 40
Janiuk, A., & Czerny, B. 2000, NewA, 5, 7
Korista, K., Baldwin, J., Ferland, G., & Verner, D. 1997, ApJS, 108, 401
Korista, K., et al. 1995, ApJS, 97, 285
Krolik, J. H., & Kallman, T. R. 1988, ApJ, 324, 714
Krolik, J. H., McKee, C. F., & Tarter, C. B. 1981, ApJ, 249, 422
Lanzetta, K. M., Turnshek, D. A., & Sandoval, J. 1993, ApJS, 84, 109
Laor, A., Bahcall, J. N., Jannuzi, B. T., Schneider, D. P., & Green, R. F. 1995, ApJS, 99, 1
Laor, A., Fiore, F., Elvis, M., Wilkes, B., & McDowell, J. C. 1997, ApJ, 477, 93
Lawrence, A., Elvis, M., Wilkes, B. J., McHardy, I., & Brandt, W. N. 1997, MNRAS, 285, 879
Lawson, A. J., & Turner, M. J. L. 1997, MNRAS, 288, 920
Leighly, K. M., Mushotzky, R. F., Nandra, K., & Forster, K. 1997, ApJ, 489, L25
Mathews, W. G., & Ferland, G. 1987, ApJ, 323, 456
Mathur, S., Elvis, M., & Singh, K. P. 1995, ApJ, 455, L9
Mathur, S., Wilkes, B., Elvis, M., & Fiore, F. 1994, ApJ, 434, 493
Moran, E. C., Halpern, J. P., & Helfand, D. J. 1996, ApJS, 106, 341
Osterbrock, D. E., & Pogge, R. W. 1985, ApJ, 297, 166
Peterson, B. M., Meyers, K. A., Capriotti, E. R., Foltz, C. B., Wilkes, B. J., & Miller, H. R. 1985, ApJ, 292, 164
Pounds, K. A., Done, C., & Osborne, J. 1995, MNRAS, 277, L5
Puchnarewicz, E. M., Mason, K. O., & Córdova, F. A. 1994, MNRAS, 270, 663
Puchnarewicz, E. M., Mason, K. O., Córdova, F. A., Kartje, J., Branduardi-Raymont, G., Mittaz, J. P. D., Murdin, P. G., & Allington-Smith, J. 1992, MNRAS, 256, 589
Puchnarewicz, E. M., Mason, K. O., Siemiginowska, A., & Pounds, K. A. 1995, MNRAS, 276, 20
Rees, M. J., Netzer, H., & Ferland, G. J. 1989, ApJ, 347, 640
Remillard, R. A., et al. 1991, Nature, 350, 589
Rodriguez-Pascual, P. M., et al. 1997, ApJS, 110, 9
Sergeev, S. G., Pronik, V. I., Malkov, Y. F., & Chuvaev, K. K. 1997, A&A, 320, 405
Shapiro, S. L., Lightman, A. P., & Eardley, D. M. 1976, ApJ, 204, 187
Shastri, P., Wilkes, B. J., Elvis, M., & McDowell, J. 1993, ApJ, 410, 29
Shuder, J. M., & Osterbrock, D. E. 1981, ApJ, 250, 55
Turnshek, D. A., Kopko, M., Monier, E., Noll, D., Espey, B. R., & Weymann, R. J. 1996, ApJ, 463, 110
Ulvestad, J. S., Antonucci, R. R. J., & Goodrich, R. W. 1995, AJ, 109, 81
Vestergaard, M., & Wilkes, B. 2000, ApJ, submitted
Wandel, A. 1997, ApJ, 490, L131
Wandel, A., & Liang, E. P. 1991, ApJ, 380, 84
Wandel, A., & Urry, C. M. 1991, ApJ, 367, 78
Wanders, I., et al. 1997, ApJS, 113, 69
Wang, T.-G., Brinkmann, W., & Bergeron, J. 1996, A&A, 309, 81
Wang, T.-G., Lu, Y.-J., & Zhou, Y.-Y. 1998, ApJ, 493, 1
Wilkes, B. J. 1999, in ASP Conf. Ser. 162, Quasars and Cosmology, ed. G. Ferland & J. A. Baldwin (San Francisco: ASP), 15
Wilkes, B. J., Elvis, M., & McHardy, I. 1987, ApJ, 321, L23
Wilkes, B. J., Kuraszkiewicz, J., Green, P. J., Mathur, S., & McDowell, J. C. 1999, ApJ, 513, 76
Witt, H. J., Czerny, B., & Życki, P. T. 1997, MNRAS, 286, 848
Wu, C.-C., Boggess, A., & Gull, T. R. 1983, ApJ, 266, 28